Rnf-213 knockout induces pericyte reduction and blood-brain barrier impairment in mouse

Wenli Sheng (shengwl@mail.sysu.edu.cn)
Sun Yat-sen University First Affiliated Hospital https://orcid.org/0000-0001-6867-371X
Wei Li
Sun Yat-sen University First Affiliated Hospital
Xingyang Niu
Sun Yat-sen University First Affiliated Hospital
Yuanyuan Dai
The Seventh Affiliated Hospital Sun Yat-sen University
Xiaoxin Wu
Sun Yat-sen University First Affiliated Hospital
Jiaoxing Li
Sun Yat-sen University First Affiliated Hospital

Research Article

Keywords: Moyamoya disease, Rnf213, pericyte, blood-brain barrier, tight junction proteins

Posted Date: February 2nd, 2023

DOI: https://doi.org/10.21203/rs.3.rs-2526175/v1

Version of Record: A version of this preprint was published at Molecular Neurobiology on July 12th, 2023.
See the published version at https://doi.org/10.1007/s12035-023-03480-y.

Abstract

Moyamoya disease (MMD) is a rare cerebrovascular disorder characterized by progressive occlusion of the internal carotid artery and the formation of an abnormal compensatory capillary network at the base of the brain. Genomics studies identified Ring finger protein 213 (RNF213) as a common genetic factor that increases the susceptibility to MMD in East Asian people. However, the function of RNF213 and its roles in pathogenesis of MMD is unclear. Here, we showed that genetic knockout of Rnf213 in mice causes significant pericytes reduction and blood-brain barrier impairment in the cortex. These phenotypes are accompanied with microglia activation and elevated level of proinflammatory cytokines. Additionally, Rnf213 deficient mice showed reduced expression of tight junction proteins, including Occludin, Claudin-5 and ZO-1. Together, these data suggested that RNF213 might contribute to the pathogenesis of MMD through disruption of pericyte homeostasis and blood-brain barrier integrity by dysregulation of inflammatory responses and tight junction formation.

Introduction

Moyamoya disease (MMD) is a rare cerebrovascular disease that significantly increases the risk of ischemic and hemorrhagic stroke in both children and adults[1–3]. MMD is characterized by chronic progressive stenosis in the terminal portions of bilateral internal carotid arteries in the circle of Willis, with compensatory development of collateral vessels network which possess a “puff of smoke” appearance and therefore termed “moyamoya vessels” in cerebral angiography[4]. The pathological characters of moyamoya vessels include intimal thickening and reduplication of the elastic lamina, partial dilatation with discontinuity of the elastic lamina, microaneurysm formation, dilative change of the vessels with medial fibrosis, and rupture of the vascular wall[5]. Recent genome-wide association analysis and exome sequencing identified ring finger protein 213 (RNF213) as one of the strongest susceptibility gene for MMD in East Asian people[6]. RNF213 is localized on chromosome 17q25.3 and encodes a 591 KDa protein that possesses a AAA-type ATPase domain, an alpha-2-macroglobulin domain, and a ring finger domain from its amino to carboxyl terminus[7]. Previous biochemistry studies revealed that the ring finger domain of RNF213 might have E3 ubiquitin ligase activity, suggesting a potential role of RNF213 in proteasome mediated degradation pathways[8, 9]. Our recent study revealed that knockout of rnf213 in zebrafish causes mulberry-like cluster of disordered-flow vascular channels, suggesting a potential role of rnf213 in cerebral cavernous formation[10]. However, the exact role of RNF213 in the pathogenesis of MMD remains unclear.

Blood-brain barrier (BBB) is a highly selective barrier, that sanctions the entry of macromolecules, cells, and pathogens from blood into the central nervous system (CNS)[11, 12]. BBB is mainly formed by vascular endothelial cells, which are sealed by continuous complexes of tight junctions[13, 14]. The function and homeostasis of BBB is also highly dependent on extracellular matrix, astrocytes and pericytes[15]. BBB disruption can lead to substantial leakage of peripheral molecules into the CNS, which might cause deleterious inflammatory and neurotoxic responses. Although the etiology of MMD remains unclear, previous studies suggested that BBB impairment might play critical roles in the pathogenesis of

MMD[16, 17]. Pathology studies showed that MMD patients has significantly higher level of BBB impairment compared to atherosclerotic cerebrovascular disease patients[18]. Importantly, recent studies indicated that RNF213 might be a key regulator of BBB integrity[19], suggesting that RNF213 might contribute to the pathogenesis of MMD through disruption of BBB integrity.

Pericytes are mural cells of brain micro-vessels uniquely positioned within the neurovascular unite (NVU) between endothelial cells, astrocytes and neurons[20]. Pericytes ensheath the capillary wall and make direct contact with vascular endothelial cells. The inter-cellular signal transduction between pericytes and vascular endothelial cells plays critical roles in maintaining key neurovascular functions of the brain, including formation and maintenance of the BBB, angiogenesis and regulation of capillary blood flow[21]. The proliferation, migration, and recruitment of pericytes to the vascular wall is controlled by endothelial-secreted platelet derived growth factor B (PDGF-BB), which binds to the platelet derived growth factor receptor beta (PDGFRβ) on pericytes to initiate downstream signaling pathways[21, 22]. Previous studies reported that the expression level of platelet derived growth factor receptor (PDGFR) was significantly reduced in MMD patient samples compared to controls[23]. Furthermore, pericyte loss and dysfunction is found in neurological disorders associated with neurovascular dysfunction and BBB breakdown, such as brain arteriovenous malformations (bAVMs)[24], cerebral cavernous malformations (CCMs)[25, 26], stroke[27], cerebral autosomal dominant arteriopathy with subcortical infarcts and leukoencephalopathy (CADASIL)[28], and microaneurysm[29]. These studies suggest that pericyte dysfunction might contribute to neurovascular diseases through disruption of BBB.

Herein, we have found that Rnf213-deficiency causes significant pericyte reduction in mouse. We propose that Rnf213 might be a key regulator of pericyte maturation and the BBB permeability.

Materials And Methods

Animals and surgery

Mice at 2-day postnatal (P2) or 3-week, and 8–10 weeks of age (body weight 20–27 grams) were used in the experiments. Mice were housed in a specific pathogen-free (SPF) environment under the condition of optimal temperature, humidity and light-dark shift cycle with food and water ad libitum. Rnf213-deficient (Rnf213(-/-)) mice on a C57BL/6 background were designed and purchased from the Laboratory Animal Center. 57BL/6 (Wild Type, WT) were purchased from experimental animal center of Sun Yat-Sen University. All strains were maintained in the condition described above. All animal experiments were performed according to the guidelines of the National Institutes of Health Guide for the Care and Use of Laboratory Animals and approved by the Sun Yat-Sen University Animal Program Animal Care and Use Committee. All animal experiments were performed in a double-blinded manner.

In vivo two-photon microscope

Age-matched mice (8–10 weeks) were exposed to the thinned-skull window preparation as described in previous studies[30]. In brief, mice were anesthetized and fixed with a custom-fabricated metal frame by

holding the head with a cyanoacrylate and dental cementon the stage of Leica DM6000 CFS (Lecia Germany) equipped with a water-immersion objective lens (25X). The skull over right somatosensory cortex was carefully thinned to ~ 20–30 μm within an area 3 mm in diameter. Imaging was performed within 30min of window construction. Data acquisition and laser scanning were performed using Leica Application Suite Advanced Fluorescence 2.5 software, at a wavelength of 860 nm. To monitor the BBB permeability using detection of leaked dyes, 100μL Rhodamine B isothiocyanate-Dextran (1.0% in saline, 70 KDa molecular weight, Sigma-Aldrich) was injected intravenously to visualize the brain vasculature. Red fluorescence channel was used for detecting the fluorescence intensity in the extravascular compartment. Images of the XYZ stacks (512 × 512 pixels) were collected to a depth of 150 μm (2-μm step size) below the cortical surface, at 5, 10, 20, 30, 45, and 60 min after the injection.

Tissue Immunofluorescence

Mice were anesthetized intraperitoneally with 100mg/kg 4% Chloral hydrate and transcardially perfused with phosphate buffer saline (PBS) and 4% paraformaldehyde separately. Brains were dissected and post-fixed in 4% paraformaldehyde for 2–6 hours. Embedded brain samples were coronally cut into 15 μm thick slices using a freezing microtome (Thermo NX50). Brain slices were blocked with 5% BSA in 0.3% Triton X-100 for 60min at room temperature and incubated with the primary antibody at 4°C overnight. To visualize brain micro-vessels in specified experiments, sections were also incubated with fluorescein-conjugated Lycopersicon esculentum lectin (LEL, TL) (Vector Laboratories, 1:200, FL-1171-1). The following primary antibodies were used: Anti-CD13 (1:200, R&D, AF2335), Anti-Iba-1 (1:200, Wako, 019-19741), Anti-GFAP (1:400, CST, 3670), Anti-ZO-1 (Affinity Biosciences, 1:200, AF5145), Anti-Claudin-5 (Affinity Biosciences, 1:200, AF5216), Anti-Occludin (Affinity Biosciences, 1:200, DF7504). After washed in PBS, brain slices were incubated with secondary antibodies (Donkey anti-Goat IgG (H + L) Cross-Adsorbed Secondary Antibody, Alexa FluorTM 555, Invitrogen, A-21432; Goat anti-Rabbit IgG (H + L;) Highly Cross-Adsorbed Secondary Antibody, Alexa FluorTM Plus 555, Invitrogen, A32732; Anti-mouse IgG (H + L), $F(ab')_2$ Fragment Alexa Fluor® 555 Conjugate, CST, 4409s; Anti-rabbit IgG (H + L), $F(ab')_2$ Fragment Alexa Fluor® 488 Conjugate, CST, 4412s) at room temperature for 1h. Slices were shielded with Fluoroshield™ and covered with glass. Images were acquired with confocal microscope (Leica DM6000 CFS) or fluorescence microscope (Nikon, Tokyo, Japan). All immunofluorescence images presented are XYZ stacks (1024 × 1024 pixels) taken by a confocal microscope, except for those in Fig. 3c.

Quantification of pericyte coverage and numbers

The quantification analysis of pericyte coverage and numbers was restricted to CD13-positive pericyte that were associated with brain capillaries defined as vessels with ≤ 6 μm in diameter, as previously described[31, 32].

For pericyte coverage, ten-micron maximum projection z-stacks (area 640 x 480 μm) were reconstructed, and the areas occupied by CD13-positive (pericyte) and lectin-positive (endothelium) fluorescent signals on vessels ≤ 6 μm were subjected separately to threshold processing and analyzed using Image J. First, black and white 8-bit images for CD13 and lectin signals were thresholded separately using Otsu's

thresholding plugin that minimize the intra-class variance of the thresholded black and white pixels. After thresholding, the integrated signal density for each thresholded image was calculated. In order to express the integrated signal density as the area of the image (in pixels) occupied by the fluorescent signal, the integrated signal density was divided by 255 (the maximum pixel intensity for an 8-bit image). The integrated pixel-based area ratios of CD13 and lectin fluorescent signals were used to determine pericyte coverage as a percentage (%) of CD13-positive surface area covering lectin-positive endothelial capillary surface area per field, as previously reported[31]. In each animal, 4–6 randomly selected fields in the somatosensory cortex S1 region (S1Cx) were analyzed in 4 nonadjacent sections (~ 100 μm apart), and averaged per mouse.

For pericyte numbers, ten-micron maximum projection z-stacks were reconstructed, and the number of CD13-positive pericyte bodies that co-localized with DAPI (4',6-diamidino-2-phenylindole)-positive nuclei on the abluminal side of lectin-positive endothelium on vessels ≤ 6μm counted using Image J Cell Counter plug-in, as previously described. In each animal, 4–6 randomly selected fields (640 x 480 μm) in the cortex, were analyzed in 4 non-adjacent sections (~ 100 μm apart), and averaged per mouse. The number of pericytes was expressed per mm^2 of tissue.

Evans Blue dye (EBD) extravasation

2% EB (3 mL/kg, Sigma) was injected via the tail vein in adult mice (8–10 weeks). 2hrs post-injection, mice were anesthetized and perfused transcardially with saline solution, followed by perfusion with 4% PFA. whole-brain samples were collected for analysis. EBD extravasation was performed as previously described[33]. Briefly, the brain specimens were weighed (wet weight of each sample was 50 mg), homogenized in 1 ml of 50% trichloroacetic acid, and centrifuged at 15,000× g for 20 minutes. 0.5 ml of the resultant supernatant was added to 1.5 ml of anhydrous ethanol. The absorbance was measured at 620nm for a colorimetric assay using a fluorescence spectrophotometer (Ex620 nm, Em680 nm) to determine the EBD concentration. The EBD content (per mg of wet weight) within the brain tissue was used to determine the BBB permeability rate of EBD. For immunofluorescence, brains were dissected and post-fixed in 4% paraformaldehyde for 2–6 hours. Embeded brain samples were coronally cut into 15 μm thick slices using a freezing microtome (Thermo NX50). Brain slices were blocked with 5% BSA in 0.3% Triton X-100 for 60min at room temperature and then using 4,6-Diamidino-2-phenylindole, dihydrochloride (DAPI, Sigma) to visualize nuclear. Slices were shielded with Fluoroshield™ and covered with glass. Images were captured with a fluorescence microscope (Nikon, Tokyo, Japan).

Western blotting

Cortex was extracted, lysed with RIPA buffer (Beyotime, P0013B) containing phosphatase inhibitor cocktail (Invitrogen, 78443), and a Pierce™ BCA Protein Assay Kit (Invitrogen, 23225) was used to quantify the protein concentration using a microplate reader. Samples were loaded and separated on 7.5% and 10% sodium dodecyl sulfate-polyacrylamide gel electrophoresis (SDS-PAGE) (EpiZyme, PG110-112, CHN), and transferred to polyvinylidene fluoride (PVDF) membranes (Millipore) according to the molecular weight of targeted protein. After blockage by 5% non-fat milk for 1 h, membranes were

incubated overnight with primary antibodies, including Anti-GAPDH (Abcam, 1:1000, ab8245, ab9425), Anti-ZO-1 (Affinity Biosciences, 1:1000, AF5145), Anti-Occludin (Affinity Biosciences, 1:1000, DF7504), Anti-Claudin-5 (Affinity Biosciences, 1:1000, AF5216), Anti-PDGF-BB (Affinity Biosciences, 1:1000, AF0240), Anti-PDGFR-β (Proteintech Group, 1:1000, 13449-1-AP), followed by incubation with appropriate HRP-conjugated secondary antibodies (1:3000) at room temperature for 1 h. An Image Quant LAS 4000 detection system (GE Healthcare Life Science, Chicago, USA) was used to visualize the target proteins on the membranes. Protein expression levels were normalized to GAPDH and quantified using Image J software.

RNA extraction and Gene Expression Analyses

Total RNA was extracted using the Trizol reagent and whole RNA was reverse transcribed and converted to complementary DNA (cDNA) through PrimeScript RT Master Mix (Takara, RR036A). Relative gene expression was evaluated by RT-qPCR (NovoStart®SYBR qPCR SuperMix plus) on real-time PCR detection system (BioRad CFX96 Touch). Relative gene expression for each target gene was calculated as the 2 (-ddct) values after normalization to the housekeeping gene (All the gene name and primer sequences were detailed as following: F-NF-kB:GCGTACACATTCTGGGGAGT, R-NF-kB: CCGAAGCAGGAGCTATCAAC. F-IL-6:CCGGAGAGGAGACTTCACAG, R-IL-6:TCCACGATTTCCCAGAGAAC. F-IL-1β:GAAGTCAAGAGAAAAGTGG, R-IL-1β:ACAGTCCAGCCCATACTTT. F-iNOS: TCCTACACCACACCAAAC, R-iNOS: CTCCAATCTCTGCCTATCC.

Statistical analysis

The Image J software (National Institutes of Health, Bethesda, MD, USA) was used to analyze the immunofluorescence results. All the data were showed in the form of mean ± SD. $P < 0.05$ is the predetermined standard of statistical significance. For BBB permeability measurements, two-way repeated measures ANOVA with Sidak's test for multiple comparisons were performed (Kress et al., 2014). For all other data, the differences between two groups were analyzed with Student's t test. All the graphs were created by GraphPad Prism 8.

Results

Pericytes reduction in cortex of Rnf213(-/-) mice

Recent studies suggested that RNF213 might regulate cerebral endothelial cell functions in vitro, and potentially control the BBB integrity[19]. To investigate the role of RNF213 in BBB-associated cell types in vivo, we generated Rnf213(-/-) mice and immuno-stained for surface markers of endothelial cell (Lectin+) and pericytes (CD13+). Confocal images were collected from coronal sections of cortex to compare pericyte number and pericyte coverage in WT and Rnf213 (-/-) mice. We found a substantial reduction of pericytes number in the cortex of Rnf213(-/-) mice compared to the corresponding age-matched WT mice. In the cortex of P2 animals, ~ 14% pericyte reduction was observed in Rnf213(-/-) mice compared to the age-matched WT (Fig. 2a, b). The difference of pericyte number between Rnf213(-/-) mice and age-

matched WT showed progressive increases with age, with 23% and 30% pericyte reduction observed in the cortex of 3-week (Fig. 2d, e), and 8–10 weeks old (Fig. 1a, c) animals, respectively. In addition, pericytes number in WT mice showed a steady trend of increase until maturity in adulthood (~ 8 weeks), while the increase of pericytes in Rnf213(-/-) mice is significantly slower compared to WT mice (SI. 1a). Consist with previous studies[34, 35], there was no difference in growth and development between Rnf213(-/-) mice and WT mice (Fig. 1b).

Consistent with the loss of pericyte number, pericyte coverage determined as a percentage (%) of CD13-positive pericyte surface area covering lectin-positive endothelial surface area (see Methods for details), showed ~ 13%, 22% and 27% reduction in the cortex of P2 (Fig. 2a, c), 3-week (Fig. 2d, f), and 8–10 weeks old (Fig. 1b, d) Rnf213(-/-) mice compared to the age-matched WT, respectively. Consistent with the quantification of pericyte number, a progressive decreased of pericyte coverage with age in the cortex of Rnf213(-/-) mice was observed. In contrast, the pericyte coverage showed no significant change at different age-stage in the age-matched WT group, (SI. 1b).

Previous literature showed that pericyte population is strictly regulated through PDGF-BB and PDGFR-β mediated signaling pathways[21]. We therefore investigated whether Rnf213 deficiency led to dysregulation of PDGF-BB and PDGFR-β levels. Western blotting analysis showed no significant difference in PDGF-BB protein levels in Rnf213 (-/-) and WT mice (Fig. 1e, f). However, the PDGFR-β protein level is significantly decreased in Rnf213 (-/-) mice (Fig. 1e, g). Together, these observations suggest that Rnf213 deficiency causes pericyte reduction, potentially through dysregulating PDGFR-β mediated pathways.

Blood-brain barrier impaired in Rnf213(-/-) mice

To further investigate whether the BBB was impaired in Rnf213 (-/-) mice, we performed in vivo time-lapse multiphoton imaging of cortical vessels with intravenous injection medium size macromolecular dextran (MW = 70,000 Da, Rhodamine B isothiocyanate-Dextran) in 8–10 weeks old Rnf213 (-/-) and age matched WT mice. In vivo time-lapse multiphoton imaging revealed that the intravascular dye began to leak into the extravascular space at the time of 10 min post-injection in 8–10 weeks old Rnf213 (-/-) mice, with the intravascular dye being accumulate in the extravascular space over time (Fig. 3a). Quantification of the tertramethylrhodamine fluorescence intensity in the extravascular compartment showed that the average fluorescence intensity in the extravascular compartment was significantly increased over the 60 mins time of observation post injection (Fig. 3b). In contrast, no intravascular dye leakage was observed in age matched WT mice at any time-point (Fig. 3a, b).

Next, we used the tail-vein injection of EBD to assess the permeability of whole cerebral vessels in 8–10 weeks old Rnf213(-/-) mice and aged matched WT. In mice injected with EBD, the uniform bluish color of the brain was observed in the Rnf213(-/-), but not WT mice (Fig. 3d). Microscopy analysis of coronal sections further revealed that EB fluorescence (red) was detected in the brain parenchyma of Rnf213 (-/-) mice (Fig. 3c). In contrast, EB retention was seen only in the endothelium (Fig. 3c) in WT animals. Measurement of EBD extravasation showed significant EBD leakage into the brain parenchyma in

Rnf213(-/-) mice but not in WT mice (Fig. 3e). Together, these data suggest that Rnf213 deficiency caused the BBB is impairment in mice.

Glial activation and elevated levels of inflammatory cytokines in Rnf213(-/-) mice

Previous literature suggested that RNF213 might regulate inflammatory responses in endothelial cells and smooth muscle cells[19, 36]. To determine whether Rnf213 deficiency causes neuroinflammation phenotypes in vivo, we immuno-stained microglia (Iba-1+) and astrocyte (GFAP+) in 8–10 weeks Rnf213(-/-) and age matched WT mice brain. Compared to WT, Rnf213(-/-) mice showed significantly increased number of Iba-1 + cells (Fig. 4a), indicating potential microglia activation in Rnf213(-/-) mice. Of note, microglia in WT mice displayed a ramified morphology with long branches and small cellular body (Fig. 4a), consistent with the previously reported morphology or resting-stage microglia[37]. In contrast, microglia in Rnf213(-/-) mice showed amoeboid morphology with a larger cellular body and shorter branches were observed, resembling the morphology of chronically activated microglia[37]. Additionally, the intensity of Iba-1 staining in Iba-1 + cells are significantly increased in Rnf213(-/-) mice compared to WT animals (Fig. 4b), further corroborating that the microglia are indeed activated in Rnf213(-/-). Consistent with the Iba-1 staining, GFAP immunostaining showed that the number of astrocytes and the density of GFAP staining are both significantly increased in Rnf213(-/-) mice compared with WT animals (Fig. 4a, c), these data suggested that Rnf213 deficiency indeed causes gliosis phenotypes in mice. Subsequently, we measured pro-inflammatory cytokines in the cortex of the Rnf213(-/-) mice. RT-qPCR revealed significantly increased level of NF-kB, IL-6, IL-1β in RNF213(-/-) mice compared to WT animals (Fig. 4d-g). These observations together showed that Rnf213 deficiency causes neuroinflammation phenotypes in mouse brains.

The expression of BBB tight junction proteins were reduced in Rnf213(-/-) mice

BBB permeability is highly dependent on the expression level of cerebrovascular endothelial tight junction proteins. Decreased expression of tight junction proteins might impair BBB integrity. We hypothesize that Rnf213 deficiency might dysregulate the expression level of key molecule in tight junction formation. We analyzed the expression of endothelial tight junction proteins in the cerebrovasculature of 8–10 weeks Rnf213 (-/-) and age-matched WT mice. Immuno-staining of tight junction proteins showed decreased level of Occludin, Claudin-5 and ZO-1 in Rnf213(-/-) mice cortex compared with WT mice (Fig. 5a-f). Consistent with the immunofluorescence-staining, analysis of protein expression using western blot showed diminished expression of Occludin, Claudin-5 and ZO-1 in the striatum of Rnf213(-/-) mice (Fig. 5g-j). These observations suggest that the expressions of tight junction proteins are reduced in Rnf213(-/-) mice.

Discussion

Recent progress in genetic association studies showed that RNF213 is a strong genetic factor for MMD. However, little is known about the exact biological function of RNF213 in the pathogenesis of MMD. In the present study, we showed that Rnf213 deficiency causes pericyte reduction, BBB impairment, glia activation, and increases pro-inflammatory cytokinesis in the cortex of Rnf213 (-/-) mice. Additionally, we demonstrated that the Rnf213 deficiency caused BBB impairment is associated with decreased expression of the tight junction proteins. Taken together, our data revealed a possible role of Rnf213 in dysregulating pericytes and BBB homeostasis, which might in-turn initiate pathogenic mechanism leading to the development of MMD.

Pericytes are known to be playing critical roles in maintaining cerebrovascular homeostasis, which are more abundant in the central nervous system compared to peripheral tissues/organs[20, 22, 38]. It was previously demonstrated that pericytes reduction can leads to endothelial hyperplasia and VEGF-A up-regulation[39]. Of note, the expression level of PDGF receptors, which plays critical roles in controlling the pericyte population, is downregulated in Moyamoya smooth muscle cells[23], indicating that the alteration in mural cell population might contribute to the pathological changes in MMD. In line with these observations, we showed that the expression level of PDGFR-β and the pericyte population are significantly decreased in Rnf213(-/-) mice, suggesting that downregulation of PDGF signaling pathway and pericyte population might contribute to the early development of RNF213 associated MMD. Of note, previous literature showed that RNF213 is an E3-ubiquitin ligase. Therefore, it is tempting to hypothesize that PDGFR-β reduction is due to the dysregulation of proteasome mediated degradation pathways. Future studies will be needed to understand the detailed molecular mechanism underlying the reduction of PDGF receptor level in RNF213 deficient animals, and to investigate whether PDGFR-β mediated pericyte loss is associated with MMD progression in human samples. Interestingly, RNF213 variants have also been linked to increased susceptibility to intracranial major arterial stenosis/occlusion(ICASO)[40], ischemic strokes[41], CCM[10] and intracranial aneurysms[42]. Previously studies suggest that pericytes loss and degeneration are also correlated with CCM[25], strokes[27], and intracranial microaneurysms[29]. These observations indicate that RNF213 might contribute to these cerebrovascular disorders through a common pathway whereby RNF213 mediated downregulation in PDGFR-β signaling pathway might result in pericyte loss and downstream pathological changes.

BBB is a specialized border selectively permits the transportation of substances from the circulating blood into the CNS. The integrity of BBB is critical to prevent toxic substances and pathogens from entering the brain[11, 12]. BBB is composed of endothelial cells connected by tight junctions, with pericytes and end-feet of astrocytes all attached to the capillary basement membrane[43]. Previous studies have demonstrated that BBB impairment is a common pathological character in cerebrovascular diseases including acute and chronic ischemia[44], cerebral small vessel disease[45], and vascular cognitive impairment[46]. In line with these studies, BBB impairment is also reported in MMD patients. Recent evidence suggests that MMD patients are more vulnerable to cerebral hyper-perfusion syndrome following a revascularization procedure[47, 48]. Although the underlying mechanism of the potential complication of revascularization procedure for MMD patients is still undetermined, it was speculated to be caused by the intrinsic fragility BBB structure in MMD patients. Interestingly, biomarker studies

showed that the expression level of matrix metalloproteinase 9 (MMP-9), a key protease controlling the degradation of the endothelial basal lamina and BBB integrity, is significantly elevated in MMD[49]. Recent studies revealed that MMP-9 expression was also significantly elevated in Rnf213(-/-) mice compared to wild-type mice after common carotid artery ligation[50]. Additionally, conditional knockout of RNF213 in brain endothelial cells showed increased BBB permeability[19]. These data suggest that RNF213 might play critical roles in BBB homeostasis. In line with these studies, our data showed that the BBB was impaired in the cortex of adult Rnf213 (-/-) mice, potentially through down-regulation of tight junction proteins in the cortex of Rnf213 (-/-) mice. This observation is consistent with recent transcriptomics and proteomics studies showing RNF213 deficiency significantly reduced tight junction protein expression[19]. Importantly, pericytes are centrally positioned in the NVU between endothelial cells, astrocytes and neurons, and maintain the integrity of BBB. Previous studies suggested that ablation of decrease in pericyte coverage dramatically damages the integrity of the BBB[38, 43]. Herein, we demonstrated that mild decrease (within 30%) of pericyte coverage caused by Rnf213 deficiency also caused significant BBB damage in mice. However, whether the pericyte loss is directly associated with the reduction of tight junction protein remained to be further investigated.

In addition to BBB damage, pro-inflammatory responses have also been implicated in the pathogenesis of MMD. Biomarker analysis using serum and cerebrospinal fluid showed significant elevation of pro-inflammatory markers in MMD patients[51–53]. Pathology studies showed that the thickened intracranial arterial intima of MMD patients contains activated macrophages and infiltrated T cells[54]. Importantly, lymphocytes accumulation within RNF213-deficient brain endothelial cell monolayers has been reported recently[19]. In line with previous studies, we showed that microglia activation and expression of pro-inflammatory cytokines are significantly elevated in Rnf213(-/-) mice. Whether the inflammatory response is the cause or the consequence of the pathological changes, including pericyte loss and BBB damage, remained to be investigated. Of note, a recent study reported that in the absence of pericytes, the NVU becomes permissive to leukocyte entry, leading to aggravated neuroinflammation which can potentially cause autoimmunity[55, 56]. Our data suggest that Rnf213 deficiency in mice may play critical roles in the initiation of the immune response through disruption of pericyte homeostasis in MMD. It would be interesting to investigate whether pericyte loss precedes NUV disruption and immune cell infiltration at the early stages of MMD in patients. Nevertheless, the currently study provided experimental evidence that warrants future studies on the potential protective effect of vascular therapies on neuroinflammation phenotypes in MMD.

In summary, our study showed the first time that Rnf213 deficiency causes significant pericytes reduction, BBB impairment, and neuroinflammation phenotypes in mice. The increased permeability of BBB might be caused by the reduction expression of the tight junction proteins in Rnf213 (-/-) mice. Thus, our findings indicate that reduction of pericytes might be a key trigger in the pathogenesis of MMD.

Abbreviations

MMD Moyamoya disease

RNF213 ring finger protein 213

BBB Blood-brain barrier

CNS central nervous system

PDGF-BB platelet derived growth factor B

bAVMs brain arteriovenous malformations

PDGFRβ platelet derived growth factor receptor beta

CADASIL cerebral autosomal dominant arteriopathy with subcortical infarcts and leukoencephalopathy

CCMs cerebral cavernous malformations

SPF specific pathogen-free

WT wild type

PBS phosphate buffer saline

EBD Evans blue dye

P2 2-day postnatal

SDS-PAGE sodium dodecyl sulfate-polyacrylamide gel electrophoresis

MMP-9 matrix metalloproteinase 9

NVU neurovascular unite

Declarations

Authors' contributions All authors contributed to the study conception and design. Material preparation, data collection and analysis were performed by Wei Li, Xingyang Niu, and Yuanyuan Dai. The first draft of the manuscript was written by Wei Li and all authors commented on previous versions of the manuscript. All authors read and approved the final manuscript.

Funding This work was funded by the National Nature Science Foundation of China (82071286, 81671132, 81471180).

Data Availability The datasets generated during and/or analyzed during the current study are available from the corresponding author on reasonable request.

Ethics Approval The procedures involving experimentation on animal subjects are reviewed and approved by the Institutional Animal Care and Use Committee, Sun Yat-Sen University (SYSU-IACUC-2022-001413).

Consent to Participate Not applicable.

Consent for Publication Not applicable.

Competing Interests The authors have no relevant financial or non-financial interests to disclose.

Acknowledgments

We would like to express the most sincere thanks to Boxing Li from Zhongshan School of Medicine, Sun Yat-sen University for comments and advice on the article.

References

1. Kuroda, S. and K. Houkin, *Moyamoya disease: current concepts and future perspectives.* Lancet Neurol, 2008. **7**(11): p. 1056-66. https://doi.org/10.1016/S1474-4422(08)70240-0
2. Scott, R.M. and E.R. Smith, *Moyamoya disease and moyamoya syndrome.* N Engl J Med, 2009. **360**(12): p. 1226-37. https://doi.org/10.1056/NEJMra0804622
3. Ihara, M., et al., *Moyamoya disease: diagnosis and interventions.* Lancet Neurol, 2022. **21**(8): p. 747-758. https://doi.org/10.1016/S1474-4422(22)00165-X
4. Suzuki, J. and A. Takaku, *Cerebrovascular "moyamoya" disease. Disease showing abnormal net-like vessels in base of brain.* Arch Neurol, 1969. **20**(3): p. 288-99. https://doi.org/10.1001/archneur.1969.00480090076012
5. Yamashita, M., K. Oka, and K. Tanaka, *Histopathology of the brain vascular network in moyamoya disease.* Stroke, 1983. **14**(1): p. 50-8. https://doi.org/10.1161/01.str.14.1.50
6. Koizumi, A., et al., *A new horizon of moyamoya disease and associated health risks explored through RNF213.* Environ Health Prev Med, 2016. **21**(2): p. 55-70. https://doi.org/10.1007/s12199-015-0498-7
7. Kamada, F., et al., *A genome-wide association study identifies RNF213 as the first Moyamoya disease gene.* J Hum Genet, 2011. **56**(1): p. 34-40. https://doi.org/10.1038/jhg.2010.132
8. Ahel, J., et al., *Moyamoya disease factor RNF213 is a giant E3 ligase with a dynein-like core and a distinct ubiquitin-transfer mechanism.* Elife, 2020. **9**. https://doi.org/10.7554/eLife.56185
9. Scholz, B., et al., *Endothelial RSPO3 Controls Vascular Stability and Pruning through Non-canonical WNT/Ca(2+)/NFAT Signaling.* Dev Cell, 2016. **36**(1): p. 79-93. https://doi.org/10.1016/j.devcel.2015.12.015
10. Lin, J., et al., *Mutations of RNF213 are responsible for sporadic cerebral cavernous malformation and lead to a mulberry-like cluster in zebrafish.* J Cereb Blood Flow Metab, 2021. **41**(6): p. 1251-1263. https://doi.org/10.1177/0271678X20914996

11. Langen, U.H., S. Ayloo, and C. Gu, *Development and Cell Biology of the Blood-Brain Barrier.* Annu Rev Cell Dev Biol, 2019. **35**: p. 591-613. https://doi.org/10.1146/annurev-cellbio-100617-062608
12. Sweeney, M.D., et al., *Blood-Brain Barrier: From Physiology to Disease and Back.* Physiol Rev, 2019. **99**(1): p. 21-78. https://doi.org/10.1152/physrev.00050.2017
13. Zlokovic, B.V., *Neurovascular pathways to neurodegeneration in Alzheimer's disease and other disorders.* Nat Rev Neurosci, 2011. **12**(12): p. 723-38. https://doi.org/10.1038/nrn3114
14. Zhao, Z., et al., *Establishment and Dysfunction of the Blood-Brain Barrier.* Cell, 2015. **163**(5): p. 1064-1078. https://doi.org/10.1016/j.cell.2015.10.067
15. Liebner, S., et al., *Functional morphology of the blood-brain barrier in health and disease.* Acta Neuropathol, 2018. **135**(3): p. 311-336. https://doi.org/10.1007/s00401-018-1815-1
16. Ren, X., et al., *Linking cortical astrocytic neogenin deficiency to the development of Moyamoya disease-like vasculopathy.* Neurobiol Dis, 2021. **154**: p. 105339. https://doi.org/10.1016/j.nbd.2021.105339
17. Lu, X., et al., *Decreased cortical perfusion in areas with blood-brain barrier dysfunction in Moyamoya disease.* Acta Neurochir (Wien), 2020. **162**(10): p. 2565-2572. https://doi.org/10.1007/s00701-020-04480-w
18. Narducci, A., et al., *In vivo demonstration of blood-brain barrier impairment in Moyamoya disease.* Acta Neurochir (Wien), 2019. **161**(2): p. 371-378. https://doi.org/10.1007/s00701-019-03811-w
19. Roy, V., et al., *Moyamoya Disease Susceptibility Gene RNF213 Regulates Endothelial Barrier Function.* Stroke, 2022. **53**(4): p. 1263-1275. https://doi.org/10.1161/STROKEAHA.120.032691
20. Winkler, E.A., R.D. Bell, and B.V. Zlokovic, *Central nervous system pericytes in health and disease.* Nat Neurosci, 2011. **14**(11): p. 1398-1405. https://doi.org/10.1038/nn.2946
21. Sweeney, M.D., S. Ayyadurai, and B.V. Zlokovic, *Pericytes of the neurovascular unit: key functions and signaling pathways.* Nat Neurosci, 2016. **19**(6): p. 771-83. https://doi.org/10.1038/nn.4288
22. Armulik, A., G. Genové, and C. Betsholtz, *Pericytes: developmental, physiological, and pathological perspectives, problems, and promises.* Dev Cell, 2011. **21**(2): p. 193-215. https://doi.org/10.1016/j.devcel.2011.07.001
23. Aoyagi, M., et al., *Development of intimal thickening in superficial temporal arteries in patients with moyamoya disease.* Clin Neurol Neurosurg, 1997. **99 Suppl 2**: p. S213-7. https://doi.org/10.1016/s0303-8467(97)00046-2
24. Winkler, E.A., et al., *Reductions in brain pericytes are associated with arteriovenous malformation vascular instability.* J Neurosurg, 2018. **129**(6): p. 1464-1474. https://doi.org/10.3171/2017.6.JNS17860
25. Wang, K., et al., *Mural Cell-Specific Deletion of Cerebral Cavernous Malformation 3 in the Brain Induces Cerebral Cavernous Malformations.* Arterioscler Thromb Vasc Biol, 2020. **40**(9): p. 2171-2186. https://doi.org/10.1161/ATVBAHA.120.314586

26. Dai, Z., et al., *Role of pericytes in the development of cerebral cavernous malformations.* iScience, 2022. **25**(12): p. 105642. https://doi.org/10.1016/j.isci.2022.105642
27. Tsao, C.C., et al., *Pericyte hypoxia-inducible factor-1 (HIF-1) drives blood-brain barrier disruption and impacts acute ischemic stroke outcome.* Angiogenesis, 2021. **24**(4): p. 823-842. https://doi.org/10.1007/s10456-021-09796-4
28. Machuca-Parra, A.I., et al., *Therapeutic antibody targeting of Notch3 signaling prevents mural cell loss in CADASIL.* J Exp Med, 2017. **214**(8): p. 2271-2282. https://doi.org/10.1084/jem.20161715
29. Lindahl, P., et al., *Pericyte loss and microaneurysm formation in PDGF-B-deficient mice.* Science, 1997. **277**(5323): p. 242-5. https://doi.org/10.1126/science.277.5323.242
30. Luo, C., et al., *Collateral blood flow in different cerebrovascular hierarchy provides endogenous protection in cerebral ischemia.* Brain Pathol, 2017. **27**(6): p. 809-821. https://doi.org/10.1111/bpa.12458
31. Bell, R.D., et al., *Pericytes control key neurovascular functions and neuronal phenotype in the adult brain and during brain aging.* Neuron, 2010. **68**(3): p. 409-27. https://doi.org/10.1016/j.neuron.2010.09.043
32. Nikolakopoulou, A.M., et al., *Regional early and progressive loss of brain pericytes but not vascular smooth muscle cells in adult mice with disrupted platelet-derived growth factor receptor-β signaling.* PLoS One, 2017. **12**(4): p. e0176225. https://doi.org/10.1371/journal.pone.0176225
33. Deng, Z., et al., *Astrocyte-derived VEGF increases cerebral microvascular permeability under high salt conditions.* Aging (Albany NY), 2020. **12**(12): p. 11781-11793. https://doi.org/10.18632/aging.103348
34. Sonobe, S., et al., *Temporal profile of the vascular anatomy evaluated by 9.4-T magnetic resonance angiography and histopathological analysis in mice lacking RNF213: a susceptibility gene for moyamoya disease.* Brain Res, 2014. **1552**: p. 64-71. https://doi.org/10.1016/j.brainres.2014.01.011
35. Kobayashi, H., et al., *Ablation of Rnf213 retards progression of diabetes in the Akita mouse.* Biochem Biophys Res Commun, 2013. **432**(3): p. 519-25. https://doi.org/10.1016/j.bbrc.2013.02.015
36. Aoyagi, M., et al., *Early development of intimal thickening in superficial temporal arteries in patients with moyamoya disease.* Stroke, 1996. **27**(10): p. 1750-4. https://doi.org/10.1161/01.str.27.10.1750
37. Savage, J.C., M. Carrier, and M. Tremblay, *Morphology of Microglia Across Contexts of Health and Disease.* Methods Mol Biol, 2019. **2034**: p. 13-26. https://doi.org/10.1007/978-1-4939-9658-2_2
38. Daneman, R., et al., *Pericytes are required for blood-brain barrier integrity during embryogenesis.* Nature, 2010. **468**(7323): p. 562-6. https://doi.org/10.1038/nature09513
39. Hellström, M., et al., *Lack of pericytes leads to endothelial hyperplasia and abnormal vascular morphogenesis.* J Cell Biol, 2001. **153**(3): p. 543-53. https://doi.org/10.1083/jcb.153.3.543
40. Miyawaki, S., et al., *Identification of a genetic variant common to moyamoya disease and intracranial major artery stenosis/occlusion.* Stroke, 2012. **43**(12): p. 3371-4. https://doi.org/10.1161/STROKEAHA.112.663864

41. Okazaki, S., et al., *Moyamoya Disease Susceptibility Variant RNF213 p.R4810K Increases the Risk of Ischemic Stroke Attributable to Large-Artery Atherosclerosis.* Circulation, 2019. **139**(2): p. 295-298. https://doi.org/10.1161/CIRCULATIONAHA.118.038439
42. Fukushima, Y., et al., *Repeated de novo aneurysm formation after anastomotic surgery: Potential risk of genetic variant RNF213 c.14576G>A.* Surg Neurol Int, 2015. **6**: p. 41. https://doi.org/10.4103/2152-7806.153709
43. Armulik, A., et al., *Pericytes regulate the blood-brain barrier.* Nature, 2010. **468**(7323): p. 557-61. https://doi.org/10.1038/nature09522
44. Yang, Y. and G.A. Rosenberg, *Blood-brain barrier breakdown in acute and chronic cerebrovascular disease.* Stroke, 2011. **42**(11): p. 3323-8. https://doi.org/10.1161/STROKEAHA.110.608257
45. Walsh, J., et al., *Microglial activation and blood-brain barrier permeability in cerebral small vessel disease.* Brain, 2021. **144**(5): p. 1361-1371. https://doi.org/10.1093/brain/awab003
46. Rajeev, V., et al., *Pathophysiology of blood brain barrier dysfunction during chronic cerebral hypoperfusion in vascular cognitive impairment.* Theranostics, 2022. **12**(4): p. 1639-1658. https://doi.org/10.7150/thno.68304
47. Fujimura, M., et al., *Significance of focal cerebral hyperperfusion as a cause of transient neurologic deterioration after extracranial-intracranial bypass for moyamoya disease: comparative study with non-moyamoya patients using N-isopropyl-p-[(123)I]iodoamphetamine single-photon emission computed tomography.* Neurosurgery, 2011. **68**(4): p. 957-64; discussion 964-5. https://doi.org/10.1227/NEU.0b013e318208f1da
48. Fujimura, M., et al., *Minocycline prevents focal neurological deterioration due to cerebral hyperperfusion after extracranial-intracranial bypass for moyamoya disease.* Neurosurgery, 2014. **74**(2): p. 163-70; discussion 170. https://doi.org/10.1227/NEU.0000000000000238
49. Kang, H.S., et al., *Plasma matrix metalloproteinases, cytokines and angiogenic factors in moyamoya disease.* J Neurol Neurosurg Psychiatry, 2010. **81**(6): p. 673-8. https://doi.org/10.1136/jnnp.2009.191817
50. Sonobe, S., et al., *Increased vascular MMP-9 in mice lacking RNF213: moyamoya disease susceptibility gene.* Neuroreport, 2014. **25**(18): p. 1442-6. https://doi.org/10.1097/WNR.0000000000000289
51. Yoshimoto, T., et al., *Evaluation of cytokines in cerebrospinal fluid from patients with moyamoya disease.* Clin Neurol Neurosurg, 1997. **99 Suppl 2**: p. S218-20. https://doi.org/10.1016/s0303-8467(97)00047-4
52. Han, W., et al., *Association of Brain-Gut Peptides with Inflammatory Cytokines in Moyamoya Disease.* Mediators Inflamm, 2020. **2020**: p. 5847478. https://doi.org/10.1155/2020/5847478
53. Han, W., et al., *Circulating sortilin levels are associated with inflammation in patients with moyamoya disease.* Metab Brain Dis, 2021. **36**(1): p. 103-109. https://doi.org/10.1007/s11011-020-00616-0
54. Masuda, J., J. Ogata, and C. Yutani, *Smooth muscle cell proliferation and localization of macrophages and T cells in the occlusive intracranial major arteries in moyamoya disease.* Stroke,

1993. **24**(12): p. 1960-7. https://doi.org/10.1161/01.str.24.12.1960

55. Török, O., et al., *Pericytes regulate vascular immune homeostasis in the CNS.* Proc Natl Acad Sci U S A, 2021. **118**(10). https://doi.org/10.1073/pnas.2016587118

56. Rustenhoven, J., et al., *Brain Pericytes As Mediators of Neuroinflammation.* Trends Pharmacol Sci, 2017. **38**(3): p. 291-304. https://doi.org/10.1016/j.tips.2016.12.001

Figures

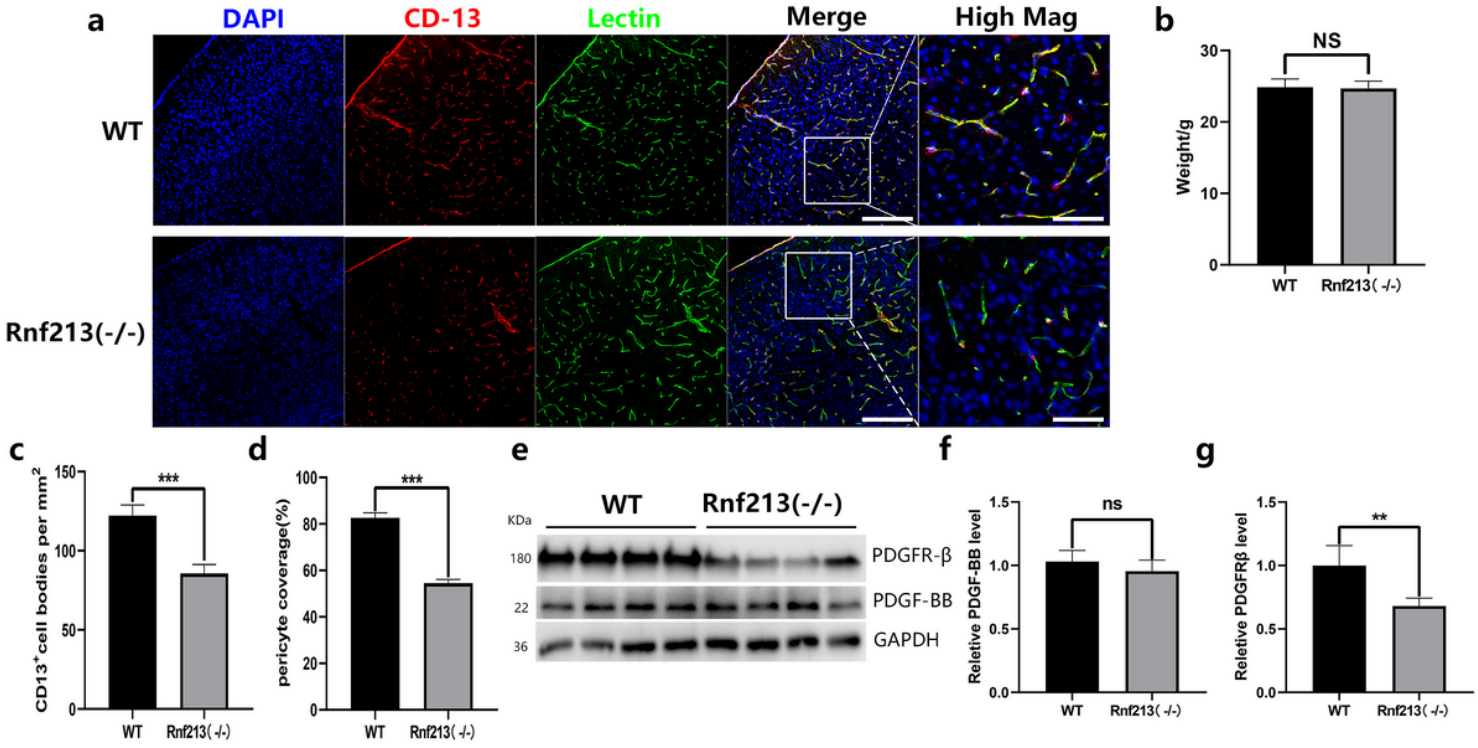

Figure 1

Pericyte reduction in the cortex of adult Rnf213 (-/-) mice.

(a) Coronal sections of cortex of 8-10 weeks Rnf213(-/-) and age matched WT mice are stained for DAPI (Blue), CD13-positive pericyte (Red) and Lectin-positive endothelial vascular cells(Green). Representative images from n=5 animals are shown. White bounding boxes are representative high magnification images of cortex sections. Scale bars represent 100 um for low-magnification images and 20 um for high-magnification images. (b) The weight of adult Rnf213(-/-) mice was not different from that of age matched WT mice. n=15 animals, NS=no significant, p>0.05. (c) Number of pericytes and (d) pericytes coverage in 8-10 weeks Rnf213 (-/-) and age matched WT mice are quantified. n=5 animals in each group are analyzed. Standard error mean is calculated. Significance is assessed using Student's t-test. ***P<0.001. (e) Brain lysates of 8-10 weeks old Rnf213-/- (n=4) and age matched WT mice (n=4) are

analyzed using SDS-page gel and immunoblotted for PDGF-BB, PDGFR-β, and GAPDH. Representative images are shown. (f) The expression level of PDGF-BB or (g) PDGFR-β was normalized to GAPDH and calculated as fold of WT. N=4 animals are quantified for each group. Standard error mean is calculated. Significance is assessed using Student's t-test. **P<0.01. ns representing no significance, P > 0.05.

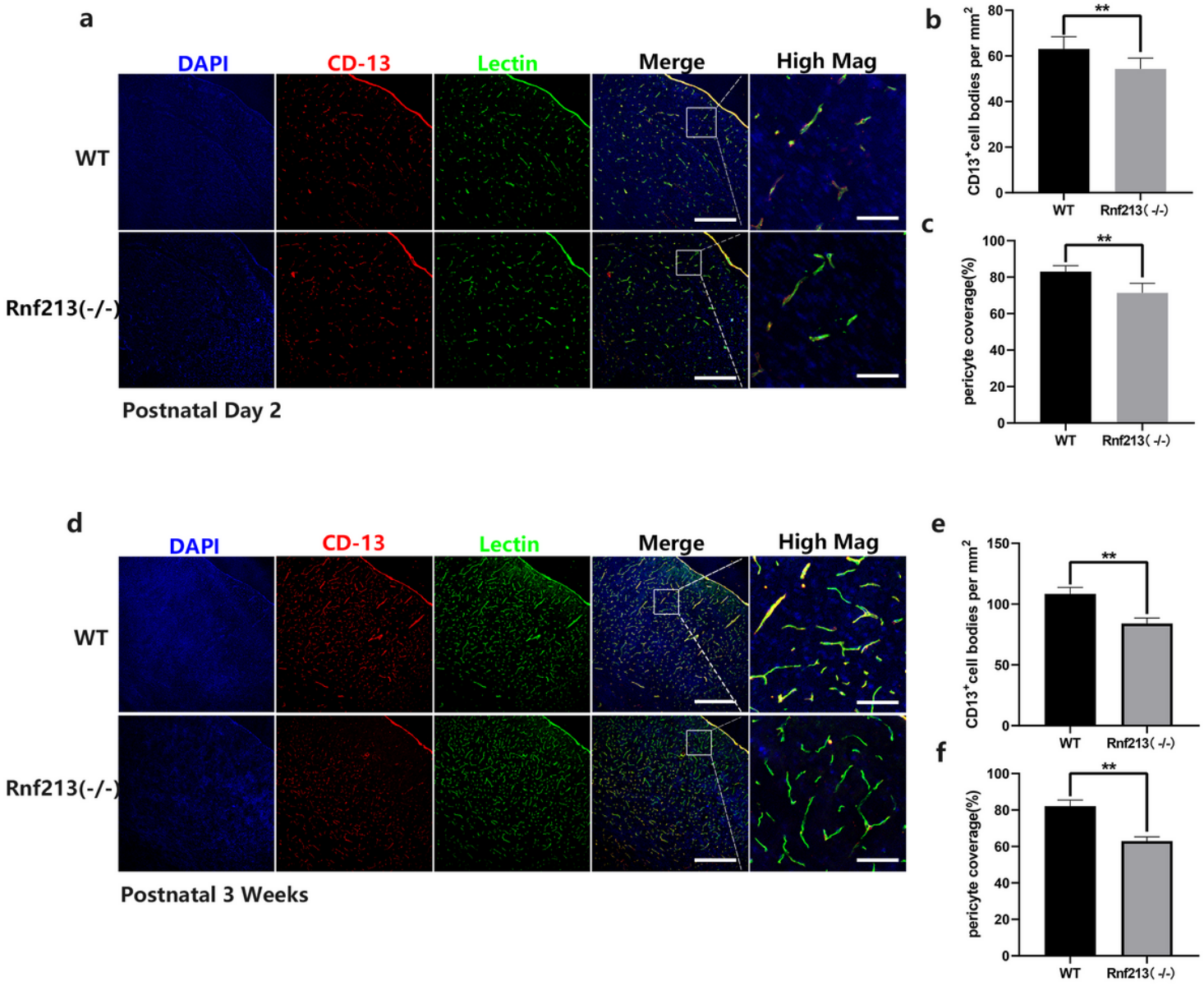

Figure 2

Pericyte reduction in cortex of P2 and 3-Week-old Rnf213 (-/-) mice.

(a) Coronal sections of cortex of P2 Rnf213-/- and age matched WT C57BL/6 mice are stained for DAPI (Blue), CD13-positive pericyte (Red) and Lectin-positive endothelial vascular cells (Green). Representative images from n=5 animals are shown. White bounding boxes are representative high magnification

images. Scale bars represent 100 um for low-magnification images and 20 um for high-magnification images. (b) Number of pericytes and (c) pericytes coverage in P2 Rnf213 (-/-) and age matched WT mice (n=5 for each group) are quantified. Standard error mean is calculated. Significance is assessed using Student's t-test. **P<0.01. (d) Coronal sections of cortex of 3-week old postnatal Rnf213 (-/-) and age matched WT C57BL/6 mice are stained for DAPI (Blue), CD13-positive pericyte (Red) and Lectin-positive endothelial vascular cells (Green). Representative images from n=5 animals for each group are shown. White bounding boxes are representative high magnification images. Scale bars represent 100 um for low-magnification images and 20 um for high-magnification images. (e) Number of pericytes and (f) pericytes coverage in 3-week old Rnf213 (-/-) and age matched WT mice (n=5 for each group) are quantified. Standard error mean is calculated. Significance is assessed using Student's t-test. **P<0.01.

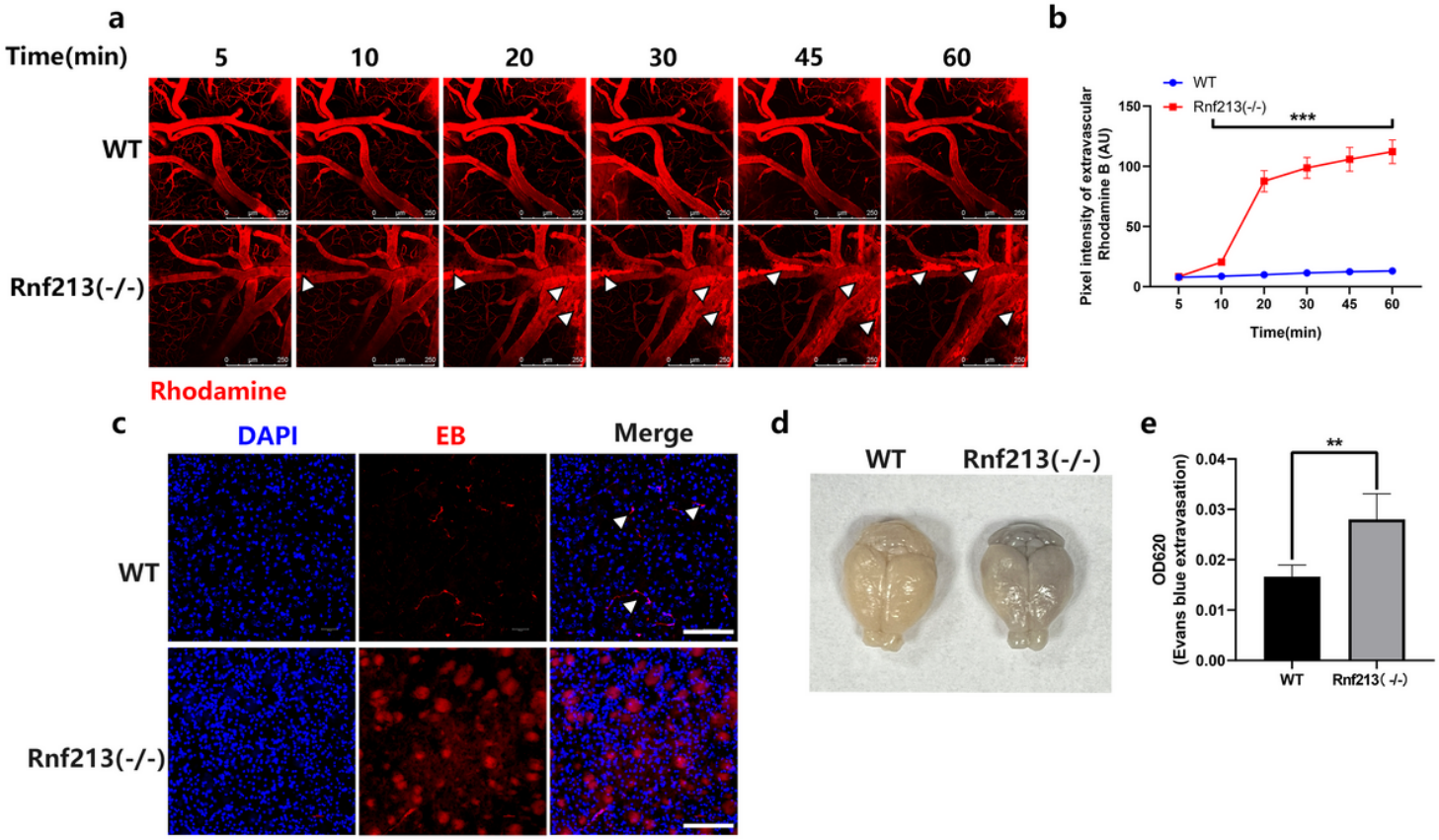

Figure 3

Blood-brain barrier broken in the cortex of RNF213(-/-) mice.

(a) Representative in vivo time-lapse multiphone imaging of tertramethylrhodamine (TMR) dextran (MW=70 KDa, Red) leakage (arrows) from cortical vessels (lay II and III, approximately 150um from the cortical surface) in 8-10 weeks old Rnf213(-/-) mouse and age matched WT mouse within 60min of TMR-dextran intravenous administration. (n=3) (b) Line diagram of the pixel intensity of extravascular Rhodamine B. (c) Representative EB fluoresence (red) is detected in the brain parenchyma after 2 h of circulation in Rnf213(-/-) mice. In control animals, EB retention is seen only in the endothelium (arrows).

(n=5). (d) Representative dissected brains of intravenously injected EB from WT (left) and Rnf213(-/-) mice (right). (n=5). Note the uniform bluish colour of the brain of the Rnf213(-/-) mice, which is absent in brains of WT mice. (e) Representative quantification of Evans blue dye extravasation into brain tissue. (n=5) Scale bar in a=250 um, Scale bar in c=20 um. **P<0.01 and ***P<0.001 versus the WT by Student's test.

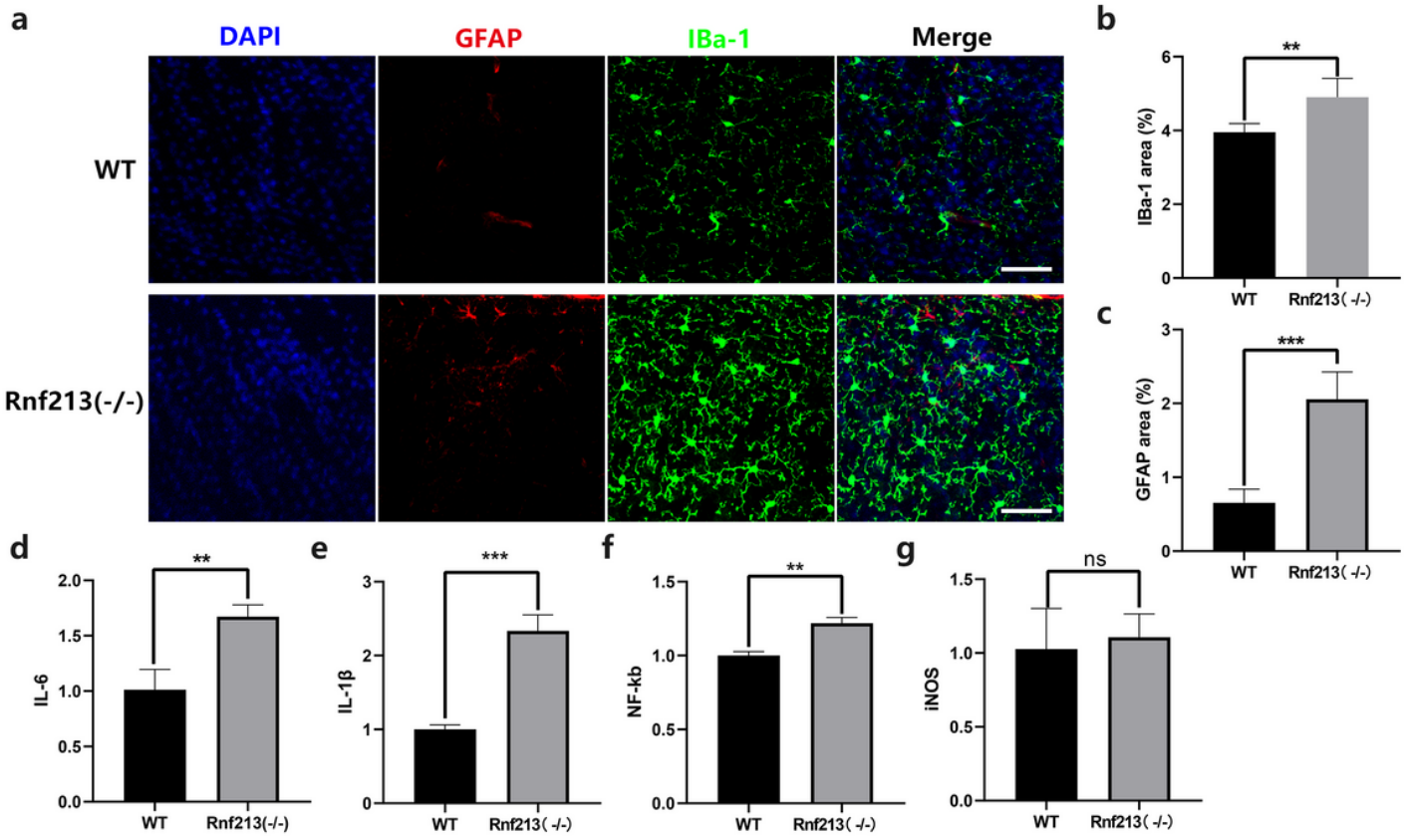

Figure 4

Glia activation and elevated levels of inflammatory cytokines in RNF213(-/-) mice

(a) Representative confocal microscope analysis of coronal sections showing DAPI (Blue), GFAP (Red), Iba-1 (Green) and merge in the cortex of 8-10 weeks old Rnf213 (-/-) and age matched WT mice. (n=5). Scale bars=20 um. (b) Proportional area of Iba-1 and (c) Proportional area of GFAP in the cortex of Rnf213 (-/-) and WT mice. (n=5). (d, e, f and g) Representative RT-qPCR analysis of mRNA levels of inflammatory cytokines genes, including IL-6, IL-1β, NF-kB, and iNOS, in the Rnf213(-/-) mice and WT mice. (n=3 per group). Data are shown as mean±S.D. **P<0.01 and ***P<0.001 versus the WT by Student's test. ns=no significance.

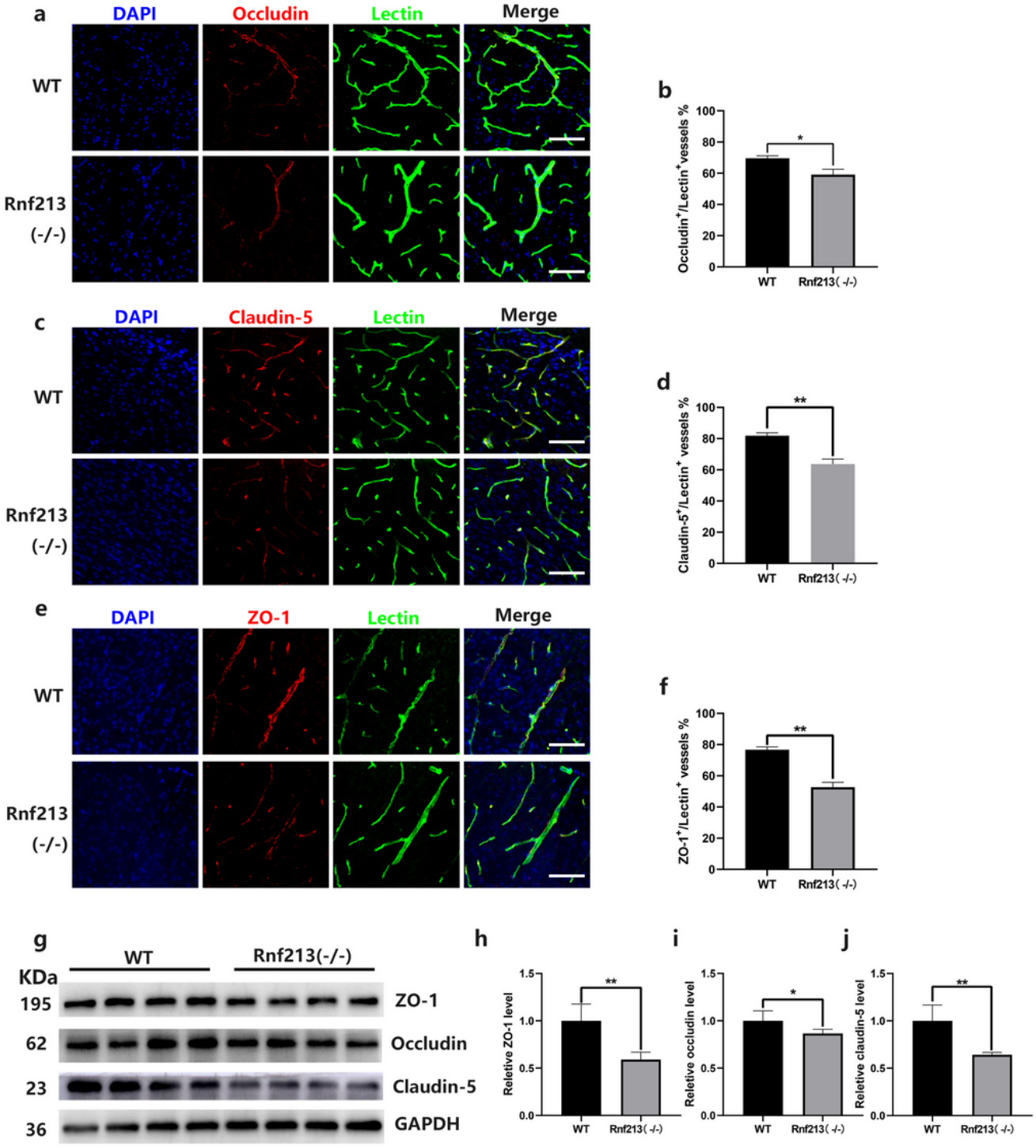

Figure 5

The expression of BBB tight junction proteins were reduced in RNF213(-/-) mice

(a, c and e) Representative confocal microscope analysis of coronal sections showing DAPI (Blue), Tight junction proteins (Red), Lectin-positive endothelial vascular profiles (Green) and merge in the cortex of 8-10 weeks old Rnf213 (-/-) and age matched WT mice. (n=5). Scale bars=20 um. (b, d and f) Quantification

of the percentage of Lectin^{+} capillaries expressing tight junction proteins (occludin, ZO-1 or claudin-5) demonstrate reduction of tight junction proteins in capillaries from Rnf213 (-/-) mice compared with those from WT mice. (g) Representative image of Western blot of ZO-1, Occludin and Claudin-5 protein levels in cortex of Rnf213 (-/-) mice and WT mice, GAPDH using cortex lysates from WT and Rnf213(-/-) mice. (h, i and j) Representative quantification analysis of ZO-1, Occludin and Claudin-5 protein levels in Rnf213 (-/-) mice and WT mice. Western blot was quantified by densitometry, all bands were normalized to GAPDH. Data are shown as mean±S.D. $^{*}P<0.05$ and $^{**}P<0.01$ versus the WT by Student's test.

Supplementary Files

This is a list of supplementary files associated with this preprint. Click to download.

- supplementaryinformation.pptx